Low temperature conduction-band transport in diamond

S. Majdi,[1,a)] M. Gabrysch,[1] K. K. Kovi,[1,2] N. Suntornwipat,[1] I. Friel,[3] and J. Isberg[1]

[1]*Division for Electricity, Department of Engineering Sciences, Uppsala University, Box 534,*
S-751 21 Uppsala, Sweden
[2]*Center for Nanoscale Materials, Argonne National Laboratory, Argonne, Illinois 60439, USA*
[3]*Element Six Innovation, Fermi Avenue, Harwell Oxford, Didcot, Oxfordshire OX11 0QR, United Kingdom*

By performing Time-of-Flight measurements on high-purity single-crystalline chemical vapor deposited diamond, we are able to extract the electron drift velocity of valley-polarized electrons in the low-injection regime. The aim of this study is to improve the understanding of the mechanisms involved in the conduction-band transport of valley-polarized electrons. The measurements were carried out within the temperature range of 10–80 K, and the experimental results are systematically compared with Monte Carlo charge transport simulations. We observe a rapid enhancement of the electron mobility with decreasing temperature, which reveals that inelastic effects in electron-phonon scattering become important below ∼40 K. In addition, we obtain the momentum relaxation rate for electrons with different valley polarizations. *Published by AIP Publishing.*
[http://dx.doi.org/10.1063/1.4964720]

Single-crystalline (SC) diamond is an extreme wide bandgap material with many exciting electrical and physical properties, making it highly desirable in power electronic applications. The key distinguishing properties of SC chemical vapor deposited (CVD) diamond are the supreme room temperature thermal conductivity,[1] the maximum breakdown field strength,[2] and the high intrinsic mobility.[3] Therefore, the SC-CVD diamond has been intensively studied for device applications aiming to utilize these extreme properties to develop new generation electronic devices. In addition, the exciting quantum mechanical properties of diamond and of various defects embedded in diamond have impelled mounting interest towards spintronic and valleytronic applications.[4,5]

The presence of defects in diamond can dramatically impact its charge transport properties such as carrier mobility, conductivity, and carrier lifetime. With decreasing temperature, the influence of lattice vibrations (phonons) on carrier scattering declines and other scattering processes, such as impurity scattering, may become dominant instead. Therefore, the study of carrier transport at low temperatures can act as a sensitive impurity scattering probe, enabling the detection of very low impurity and defect concentrations. Hall-effect measurements cannot be applied to measure the mobility or drift velocity in the case of insulating or highly resistive materials, such as high purity intrinsic diamond. Photo-Hall measurements can be carried out for highly resistive materials, but this method gives a non-equilibrium carrier distribution, which complicates the interpretation. Photo-Hall measurements on diamond at temperatures down to 10 K on boron and phosphorus-doped diamond have been reported previously.[6,7] The Time-of-Flight (ToF) method is especially suitable for carrier velocity measurements at very low carrier concentrations and for highly resistive materials. In diamond, electron-hole pairs can be created by α-particles,[8–10] pulsed

electron beams,[11] pulsed particle beams,[12] pulsed X-rays,[13] or using a Q-switched UV laser.[3,14–16]

In diamond, at temperatures above ∼150 K, the drift velocities of electrons and holes as functions of the applied electric field exhibit a very similar behavior.[17–21] For both carrier types, a linear relation between drift velocity and electric field holds for low fields, whereas with increasing field, a saturation of the velocity occurs. Below ∼150 K, this resemblance disappears, and electrons and holes exhibit a very different behavior. The difference originates in the completely different structure of the valence and conduction bands in diamond. The conduction band of diamond consists of six isolated energy minima (valleys) on the Δ-axis in the Brillouin zone. The energy surface for an energy slightly above the minimum forms six ellipsoids. Within the temperature interval of 110–150 K, repopulation effects between the valleys give rise to a negative differential mobility.[22] Below 80 K, the intervalley scattering rate resulting from phonon interactions becomes so low $(<10^4\,\mathrm{s}^{-1})$[23] that electrons are effectively confined to a given valley. With an electric field applied along the [100] direction, electrons in the two valleys on the (100) axis will respond to the field with the longitudinal effective mass (m_l) while electrons in the four other valleys respond with the smaller transversal effective mass (m_t). Since $m_t < m_l$, electrons in the four latter valleys obtain a higher carrier temperature, and in the following, we will denote these four valleys as "hot" valleys and the other two valleys as "cool" valleys.[5]

Quite differently from the structure of the conduction band, the valence band consists of three bands having their maxima at the Γ point: the heavy-hole (*hh*), light-hole (*lh*), and split-off (*so*) bands. The drift velocity of holes at low temperatures has been discussed and investigated in a previous work.[24] In this letter, we investigate the transport of valley-polarized electrons in the conduction-band, which is important for the realization of valley-based information processing and valley-based quantum computing.[25,26]

a)Author to whom correspondence should be addressed. Electronic mail: Saman.Majdi@angstrom.uu.se

Here, we apply the ToF technique and demonstrate that it is possible to measure the drift velocity of electrons down to 10 K for very low electric fields, well below 10 V/cm. In addition, we compare our data to Monte Carlo (MC) simulations to identify the dominating scattering mechanisms and discuss the effects of carrier heating and inelastic phonon-electron scattering. We also determine the momentum relaxation rate for electrons with different valley polarizations as a function of temperature. As pointed out in earlier studies,[27,28] the spin relaxation time for conduction band electrons is intimately related to the momentum relaxation time whenever spin relaxation is governed by the Elliott-Yafet mechanism. Therefore, this result is also important for spintronics.

A set of freestanding single-crystalline CVD diamond plates was synthesized under conditions of high purity by Element Six, Ltd. The samples were deposited homoepitaxially on specially prepared high-pressure high-temperature (HPHT) synthetic diamond substrates in a microwave plasma-assisted CVD reactor. To produce the freestanding plates, the epitaxial overlayers were separated from their HPHT diamond substrate by laser cutting and then polished. The samples are 4.5×4.5 mm, with thicknesses 510 and 690 μm and a nitrogen impurity concentration below 5×10^{14} cm^{-3}.

In the ToF measurements, the CVD diamond samples were illuminated using a passively Q-switched UV laser delivering 800 ps (FWHM) pulses with a wavelength of 213 nm at a repetition rate of 300 Hz. The light is focused onto the sample surface at a circular spot with a diameter of 2 mm. A low-noise broadband current amplifier (1 GHz, 24 dB) together with a digital storage oscilloscope (DSO) is used, and the bias is applied using a 50 μs pulser via a bias-tee. The pulsed bias ensures capacitive voltage distribution across the sample and avoids undesirable sample charging. Several interference filters guarantee a pure 213 nm spectral output, and neutral density filters allow for reducing the intensity to any desired level. Ti/Al (20/300 nm) semitransparent mesh contacts (Ø 3 mm) were deposited on the two opposite (100) faces of the samples. The contact geometry makes it possible to apply a homogenous electric field. Electron-hole pairs are created near (within a few micrometers) the illuminated surface of the sample due to the strong absorption of the 213 nm light in diamond. The temperature was monitored using a LakeShore 331 temperature controller with a calibrated TG-120-CU-HT-1.4 H GaAlAs diode sensor. The samples were mounted on a ceramic chip carrier and placed in a liquid helium cooled vacuum cryostat with UV optical access.

For the MC simulations, we use a simple conduction band structure, consisting of six parabolic but anisotropic (ellipsoidal) valleys. This simplification is adequate at the moderate electric fields considered in this work, and it reduces the computational effort considerably, compared to full-band simulations. Here, we consider scattering with acoustic phonons, and this is treated through inelastic deformation-potential interaction. Optical phonon scattering can be neglected at the temperatures and electric fields that we consider in this study. Additionally, the impact of impurity scattering in the ultrapure samples ((*impurity concentration* $< 10^{14}$ cm^{-3})[19] and (*ionized impurity concentration* $< 10^{12}$ cm^{-3})[24]) used here is

expected to be quite small. In a crystal with the valleys centered on the {100} axes, the deformation potential tensor has two independent components for interactions with the transversal and longitudinal phonon modes. However, the effect of this anisotropy is not large,[29] and as a further simplification, it is possible to average over the phonon wave vector angle, which leaves only one independent component of the deformation potential tensor. With these simplifications, the acoustic phonon scattering rate P_{ac} can be written[30]

$$P_{ac}(\mathbf{k}, \mathbf{k} \pm \boldsymbol{\kappa}) = \frac{q\pi D_A^2}{V\rho v} \left\{ \left(\exp\left(\frac{\hbar v\kappa}{kT}\right) - 1 \right)^{-1} + \frac{1}{2} \mp \frac{1}{2} \right\}$$
$$\cdot \delta(E_c(\mathbf{k} \pm \boldsymbol{\kappa}) - E_c(\mathbf{k}) \mp \hbar v\kappa), \quad \kappa = |\boldsymbol{\kappa}|, \tag{1}$$

where $\boldsymbol{\kappa}$ is the phonon wave vector and $\mathbf{k}$ and $\mathbf{k} \pm \boldsymbol{\kappa}$ are the initial and final state electron wave vectors, respectively. V is the crystal volume, and ρ is the material density (3.515 g/cm^3). The upper sign is taken for phonon absorption and the lower sign for phonon emission. v is an averaged sound velocity $v = (2v_t + v_l)/3$.[30] For diamond, the longitudinal acoustic velocity v_l is 17.52 km/s, and the transversal acoustic velocity v_t equals 12.82 km/s.[31]

The acoustic deformation potential D_A is assumed to be $D_A = 11.5$ eV, which gave the best results within the limits given in Ref. 23. For the effective masses, we use the values: longitudinal effective mass $m_l/m_0 = 1.56$ and transversal effective mass $m_t/m_0 = 0.28$.[32] In the final state selection in the MC simulation, we keep the treatment described in Ref. 30. For a parabolic ellipsoidal band, it is possible to give closed expressions for the longitudinal and transversal mobilities. The derivation is quite similar to the usual derivation of acoustic deformation potential scattering in a spherical band.[33] Integrating Eq. (1) over the phonon population, assuming a linear phonon dispersion (so that the phonon density-of-states (DOS) equals $\frac{\kappa^2}{2\pi^2 v_{l,t}}$), yields the averaged electron-phonon scattering rates for phonon absorption (Γ_{ab}) and phonon emission (Γ_{em})[33]

$$\Gamma_{ab,em} = \frac{m_{dos}^{1/2} D_A^2}{2^{5/2}\pi\,\hbar^4\rho v^4}(kT)^3 E_c^{-1/2}$$
$$\times \int \kappa^2 \left(\frac{1}{\exp(\hbar v\kappa/kT) - 1} + \frac{1}{2} \mp \frac{1}{2} \right) d\kappa, \tag{2}$$

where, as before, the upper sign is taken for phonon absorption and the lower sign for phonon emission. The density-of-states effective mass is $m_{dos} = m_l^{1/3} m_t^{2/3}$, and E_c is the electron energy in the ellipsoidal valley. The integration is extended over all values of κ that are consistent with energy and momentum conservation. The relaxation time τ is obtained as a weighted energy average over the carrier distribution[34]

$$\tau = \frac{4}{3\sqrt{\pi}}(kT)^{-5/2} \int_0^\infty \frac{E_c^{3/2}}{\Gamma_{ab}(E_c) + \Gamma_{em}(E_c)} \exp(-E_c/kT) dE_c \tag{3}$$

and the longitudinal/transverse mobilities are given by $\mu_{l,t} = \frac{q\tau}{m_{l,t}}$. At high temperatures, when the (root mean square)
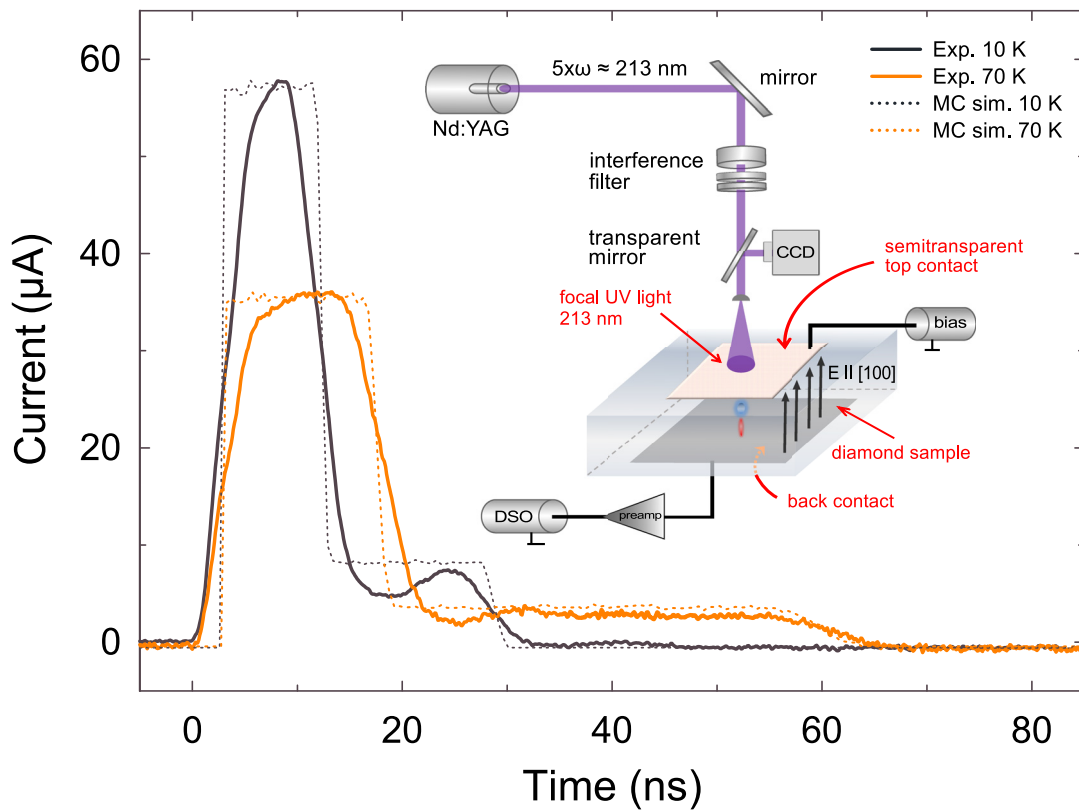
FIG. 1. Current traces measured at 10 K and 70 K for 135 V/cm compared with simulations. Inset: Schematics of the Time-of-Flight setup and sample configuration used in the measurement.

thermal velocity of the electrons $v_{th} = \sqrt{kT(2/m_t + 1/m_l)}$ is much larger than the sound velocity ($v_{th} \gg v$) electron-phonon scattering is nearly elastic, the absorption and emission rates become equal, and the integral in Eq. (2) approximately yields the simple $\mu \propto T^{-3/2}$ relation

$$\mu_{l,t} = \frac{4q\sqrt{\pi}\hbar^4 \rho \nu^2}{3\sqrt{2}D_A^2 m_{l,t} m_{dos}^{3/2}} (kT)^{-3/2}. \qquad (4)$$

By fitting error-functions to the rising and falling edges of the measured current pulse in the ToF experiment, the transit time of the electrons can be determined using the procedure described previously.[35] For illustration, the current traces measured for two temperatures (10 and 70 K) for one of the samples are plotted in Fig. 1.

The drift velocity v_d is given by the quotient of the sample thickness and the transit time. A strong non-ohmic behavior (i.e., deviation from a simple linear $v_d = \mu E$ relation, where μ is the low-field drift mobility and E the electric field strength) can be observed (Fig. 2), especially at low lattice temperatures (T_L) and high electric fields E. It is clear from the MC simulation that this is due to the carrier heating by the electric field, i.e., the carrier temperature (T_C) becomes substantially larger than T_L. In contrast, for the low electric fields, below about 100 V/cm at 80 K or below about 20 V/cm at 20 K, carrier heating is negligible, and we observe ohmic behavior.

Hence, the carrier mobilities can be extracted (separately for cool and hot valleys). These are plotted as a function of T_L in Fig. 3. In the simplest treatment of deformation potential
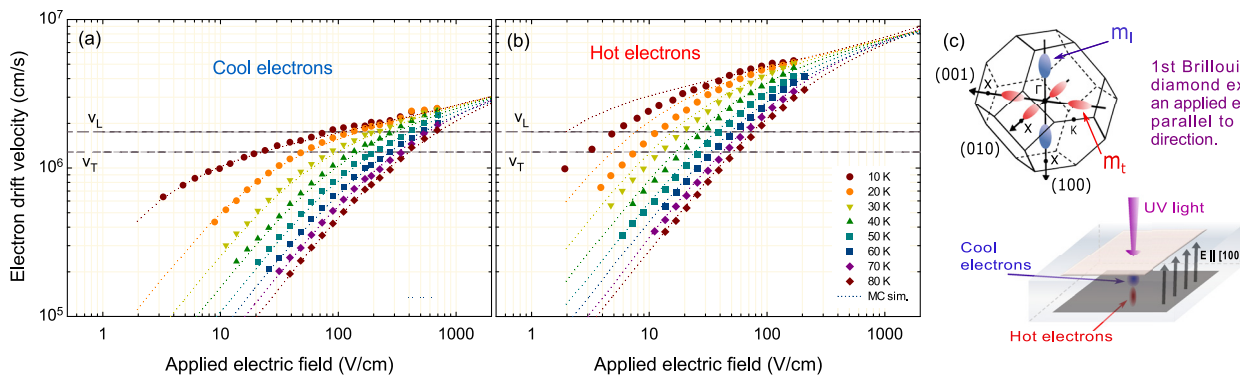

FIG. 2. Comparison of experimental (a) cool and (b) hot electron drift velocity, in the temperature range $T_L = 10$–80 K, with MC simulations. The dotted lines are traces from the MC simulations. Dashed lines indicate the longitudinal and transversal sound velocities in diamond. (c) The schematic of the electron transport inside the diamond sample and the 1st Brillouin zone under applied bias where an inhomogeneous heating of electrons in the orthogonal valleys ($m_t < m_l$) takes place.
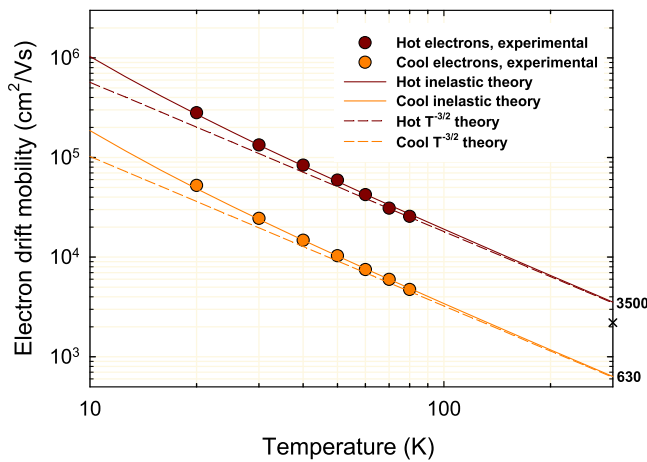
FIG. 3. Experimental low-field drift electron mobilities (circles) as a function of temperature compared with inelastic theory for deformation potential scattering (solid lines) and with the $T^{-3/2}$ behavior obtained from the elastic approximation (dashed lines). The cross indicates the measured electron mobility at 300 K.

scattering of electrons and acoustic phonons, it is customary to ignore the electron-phonon energy exchange. This elastic approximation leads to the $\mu \propto T^{-3/2}$ law (Eq. (4)) for the temperature dependence of the mobility, which agrees well with measurements on diamond at 80–300 K. At higher temperatures than ~300 K, the mobility decreases more rapidly due to the onset of optical phonon scattering.

We observe a clear deviation from the $T^{-3/2}$ law at temperatures well below 80 K, as can be seen in Fig. 3. The measured mobilities are substantially higher than the $T^{-3/2}$ law states. This can be attributed to the breakdown of the elastic (or high-temperature) approximation.[33] In absorbing (emitting) a phonon, the electron gains (loses) energy, which in turn leads to an increase (decrease) in the number of available electron states to scatter into. This shift in the density of states becomes more pronounced at low carrier energies, and therefore at low temperatures. Actually, if the carrier velocity falls below the velocity of sound in the medium, the phonon emission is no longer possible at all, since there are no available states to scatter into. That is, only supersonic electrons can emit phonons (cf. e.g., sonic booms or Čerenkov radiation). Thus, at low velocities, only phonon *absorption* is available as a process for scattering, resulting in a strong enhancement in both the transversal and longitudinal electron mobilities at low temperature. However, the deviation between the observed experimental data and MC simulation for hot valley electrons at the lowest temperatures indicates some influence of impurity scattering.

Taking the inelastic nature of electron-phonon scattering into account, Eq. (3) reproduces the experimental mobilities very well, as indicated in Fig. 3. As a further verification, the MC simulations that incorporate inelastic electron-phonon scattering (using Eq. (1) for the scattering rate) also produce exactly the same behavior. Thus, the experimental data constitute a clear observation of inelastic electron-acoustic phonon scattering in diamond. This effect was observed in exciton diffusion[32] but has not previously been observed for free carriers in a drift velocity measurement in any semiconductor. The observation of this effect is made possible in

diamond due to the combination of having a high-purity material (with low impurity scattering rates) and a material with a uniquely high sound velocity.

By extrapolating to 300 K, the hot and cool electron mobilities measured below 80 K as in Fig. 3 we find $\mu_{hot} = 3500 \, cm^2/Vs$ and $\mu_{cool} = 630 \, cm^2/Vs$. This combines to an effective mobility (for equipopulated valleys) $\mu_{eff} = \frac{2}{3} \mu_{hot} + \frac{1}{3} \mu_{cool} = 2540 \, cm^2/Vs$. At 300 K, we measure $\mu_{eff} = 2200 \, cm^2/Vs$, a slightly lower value, but this difference can conceivably be explained by the beginning onset of optical phonon scattering at room temperature, giving a small additional reduction in mobility. The 300 K mobility is in good agreement with some previously observed values.[19,36] By time-resolved cyclotron resonance measurements, Naka *et al.* find much higher mobilities in SC diamond, e.g., $5.1 \times 10^5 \, cm^2/Vs$, $2 \times 10^5 \, cm^2/Vs$ at 20 respective 40 K and $7.3 \times 10^3 \, cm^2/Vs$ at 300 K by the same $T^{-3/2}$ extrapolation. This is claimed[37] to be related to the longer momentum relaxation times, estimated in ultrapure diamond samples with a carrier concentration below $10^{11} \, cm^{-3}$.

From the measured mobilities, it is possible to determine the momentum relaxation rate (for electrons in different valleys separately). This was done by adjusting the relaxation time in the MC simulation so as to reproduce the observed values of mobility. The result is plotted in Fig. 4. It can be noted that the momentum relaxation time is essentially the same in both hot and cool valleys.

To summarize, we have studied the electron drift velocity in high quality single-crystalline diamond using Time-of-Flight measurements in the [100] direction. The experimental observations were compared with Monte Carlo simulations. We can distinguish two types of electron valley polarizations (hot and cool) due to the broken cubic symmetry in the presence of an applied electric field. A non-ohmic behavior was observed within the measured temperature interval 10–80 K, which can be explained by carrier heating and this could be reproduced in Monte Carlo simulations. At very low electric fields, the velocity is linear in electric field, and we were able to obtain the electron mobilities for hot and cool valleys down to 20 K. At the lowest temperatures, the measured mobilities
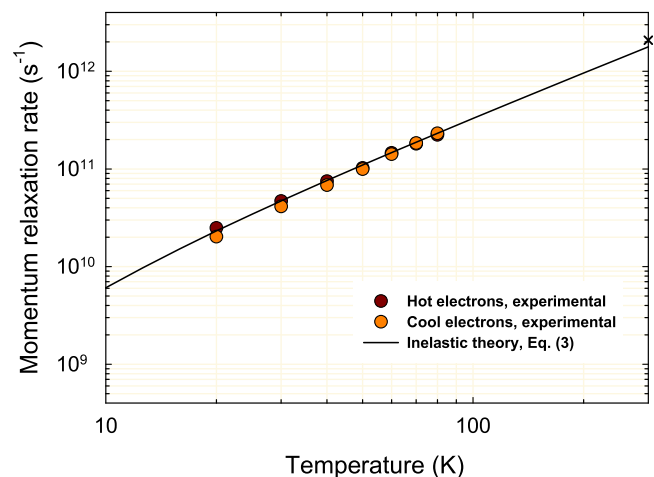

FIG. 4. Values of the momentum relaxation rate obtained by comparing drift mobility data with the MC simulations. The cross indicates the momentum relaxation rate at 300 K.

are substantially higher than the simple $T^{-3/2}$ law states. This was attributed to the breakdown of the elastic approximation of electron-acoustic phonon scattering in diamond and the effect of inelastic scattering has not previously been directly observed for free carriers in a drift velocity measurement in any semiconductor. By comparing mobility data to Monte Carlo simulations, it was also possible to obtain values for the momentum relaxation time of valley-polarized electrons.

[1]S. Barman and G. P. Srivastava, J. Appl. Phys. **101**, 123507 (2007).

[2]C. A. Klein and R. DeSalvo, Appl. Phys. Lett. **63**, 1895 (1993).

[3]J. Isberg, J. Hammersberg, E. Johansson, T. Wikström, D. J. Twitchen, A. J. Whitehead, S. E. Coe, and G. A. Scarsbrook, Science **297**, 1670 (2002).

[4]J. Cardellino, N. Scozzaro, M. Herman, A. J. Berger, C. Zhang, K. C. Fong, C. Jayaprakash, D. V. Pelekhov, and P. C. Hammel, Nat. Nanotechnol. **9**, 343 (2014).

[5]J. Isberg, M. Gabrysch, J. Hammersberg, S. Majdi, K. K. Kovi, and D. Twitchen, Nat. Mater. **12**, 760 (2013).

[6]Z. Remes, R. Kalish, C. Uzan-Saguy, E. Baskin, M. Nesládek, and S. Koizumi, Phys. Status Solidi A **199**, 82 (2003).

[7]Z. Remes, C. Uzan-Saguy, E. Baskin, R. Kalish, Y. Avigal, M. Nesladek, and S. Koizumi, Diamond Relat. Mater. **13**, 713 (2004).

[8]H. Pernegger, S. Roe, P. Weilhammer, V. Eremin, H. Frais-Kölbl, E. Griesmayer, H. Kagan, S. Schnetzer, R. Stone, W. Trischuk, D. Twitchen, and A. Whitehead, J. Appl. Phys. **97**, 073704 (2005).

[9]S. Gkoumas, A. Lohstroh, and P. J. Sellin, Diamond Relat. Mater. **18**, 1338 (2009).

[10]M. Pomorski, E. Berdermann, A. Caragheorgheopol, M. Ciobanu, M. Kiš, A. Martemiyanov, C. Nebel, and P. Moritz, Phys. Status Solidi A **203**, 3152 (2006).

[11]G. Ottaviani, C. Canali, F. Nava, and J. W. Mayer, J. Appl. Phys. **44**, 2917 (1973).

[12]L. S. Pan, S. Han, D. R. Kania, S. Zhao, K. K. Gan, H. Kagan, R. Kass, R. Malchow, F. Morrow, W. F. Palmer, C. White, S. K. Kim, F. Sannes, S. Schnetzer, R. Stone, G. B. Thomson, Y. Sugimoto, A. Fry, S. Kanda, S. Olsen, M. Franklin, J. W. Ager, and P. Pianetta, J. Appl. Phys. **74**, 1086 (1993).

[13]M. Gabrysch, E. Marklund, J. Hajdu, D. J. Twitchen, J. Rudati, A. M. Lindenberg, C. Caleman, R. W. Falcone, T. Tschentscher, K. Moffat, P. H. Bucksbaum, J. Als-Nielsen, A. J. Nelson, D. P. Siddons, P. J. Emma, P. Krejcik, H. Schlarb, J. Arthur, S. Brennan, J. Hastings, and J. Isberg, J. Appl. Phys. **103**, 64909 (2008).

[14]L. S. Pan, D. R. Kania, P. Pianetta, J. W. Ager III, M. I. Landstrass, and S. Han, J. Appl. Phys. **73**, 2888 (1993).

[15]N. Tranchant, M. Nesladek, D. Tromson, Z. Remes, A. Bogdan, and P. Bergonzo, Phys. Status Solidi A **204**, 3023 (2007).

[16]Y. Oshiki, J. H. Kaneko, F. Fujita, A. Homma, H. Watanabe, K. Meguro, Y. Yamamoto, T. Imai, K. Sato, K. Tsuji, S. Kawamura, and M. Furusaka, Diamond Relat. Mater. **17**, 833 (2008).

[17]J. Pernot, P. N. Volpe, F. Omnès, P. Muret, V. Mortet, K. Haenen, and T. Teraji, Phys. Rev. B: Condens. Matter Mater. Phys. **81**, 205203 (2010).

[18]M. Pomorski, E. Berdermann, M. Ciobanu, A. Martemyianov, P. Moritz, M. Rebisz, and B. Marczewska, Phys. Status Solidi A **202**, 2199 (2005).

[19]M. Gabrysch, S. Majdi, D. J. Twitchen, and J. Isberg, J. Appl. Phys. **109**, 63719 (2011).

[20]F. Nava, C. Canali, C. Jacoboni, L. Reggiani, and S. F. Kozlov, Solid State Commun. **33**, 475 (1980).

[21]L. Reggiani, S. Bosi, C. Canali, F. Nava, and S. F. Kozlov, Phys. Rev. B **23**, 3050 (1981).

[22]J. Isberg, M. Gabrysch, S. Majdi, and D. Twitchen, Appl. Phys. Lett. **100**, 172103 (2012).

[23]J. Hammersberg, S. Majdi, K. K. Kovi, N. Suntornwipat, M. Gabrysch, D. J. Twitchen, and J. Isberg, Appl. Phys. Lett. **104**, 232105 (2014).

[24]S. Majdi, K. K. Kovi, J. Hammersberg, and J. Isberg, Appl. Phys. Lett. **102**, 152113 (2013).

[25]O. Gunawan, Y. P. Shkolnikov, K. Vakili, T. Gokmen, E. P. De Poortere, and M. Shayegan, Phys. Rev. Lett. **97**, 186404 (2006).

[26]G. Y. Wu, N.-Y. Lue, and L. Chang, Phys. Rev. B **84**, 195463 (2011).

[27]N. Naka, K. Fukai, Y. Handa, and I. Akimoto, J. Lumin. **152**, 93 (2014).

[28]O. D. Restrepo and W. Windl, Phys. Rev. Lett. **109**, 166604 (2012).

[29]E. M. Conwell, "High field transport in semiconductors," in *Solid State Physics*, edited by F. Seitz, D. Turnbull, and H. Ehrenreich (Academic Press, New York, 1967).

[30]C. Jacoboni and L. Reggiani, Rev. Mod. Phys. **55**, 645 (1983).

[31]S. Koizumi, C. Nebel, and M. Nesladek, *Physics and Applications of CVD Diamond* (John Wiley & Sons, 2008).

[32]N. Naka, K. Fukai, Y. Handa, and I. Akimoto, Phys. Rev. B **88**, 35205 (2013).

[33]D. P. Trauernicht and J. P. Wolfe, Phys. Rev. B **33**, 8506 (1986).

[34]M. Lundstrom, *Fundamentals of Carrier Transport*, 2nd ed. (Cambridge University Press, Cambridge, 2000).

[35]J. Isberg, S. Majdi, M. Gabrysch, I. Friel, and R. Balmer, Diamond Relat. Mater. **18**, 1163 (2009).

[36]M. Nesladek, A. Bogdan, W. Deferme, N. Tranchant, and P. Bergonzo, Diamond Relat. Mater. **17**, 1235 (2008).

[37]I. Akimoto, Y. Handa, K. Fukai, and N. Naka, Appl. Phys. Lett. **105**, 32102 (2014).